

# Medical image restoration of dynamic lungs using optical transfer function of lung motion

## D. Arbel

Ben-Gurion University of the Negev  
Electrical and Computer Engineering Department  
Beer-Sheva 84105, Israel

## O. Hadar

Ben-Gurion University of the Negev  
Communication Systems Engineering Department  
Beer-Sheva 84105, Israel

## N. S. Kopeika

Ben-Gurion University of the Negev  
Electrical and Computer Engineering Department  
Beer-Sheva 84105, Israel

**Abstract.** When carrying out medical imaging based on detection of isotopic radiation levels of internal organs such as lungs or heart, distortions, and blur arise as a result of the organ motion during breathing and blood supply. Consequently, image quality declines, despite the use of expensive high resolution devices and, such devices are not exploited fully. A method with which to overcome the problem is image restoration. Previously, we suggested and developed a method for calculating numerically the optical transfer function (OTF) for any type of image motion. The purpose of this research is restoration of original isotope images (of the lungs) by restoration methods that depend on the OTF of the real time relative motion between the object and the imaging system. This research uses different algorithms for the restoration of an image, according to the OTF of the lung motion, which is in several directions simultaneously. One way of handling the three-dimensional movement is to decompose the image into several portions, to restore each portion according to its motion characteristics, and then to combine all the image portions back into a single image. An additional complication is that the image was recorded at different angles. The application of this research is in medical systems requiring high resolution imaging. The main advantage of this approach is its low cost versus conventional approaches. © 2001 Society of Photo-Optical Instrumentation Engineers. [DOI: 10.1117/1.1352749]

Keywords: lung motion; image motion; image vibration; image restoration; optical transfer function; medical imaging; isotope imaging.

Paper 20001 received Feb. 9, 2000; revised manuscript received Dec. 6, 2000; accepted for publication Dec. 11, 2000.

## 1 Introduction

Ventilation studies are clinically useful for evaluating lung function. By quantizing ventilation studies, we are able to evaluate the degree of ventilatory dysfunction, evaluate the response to therapy, and assess the relationship between ventilation and perfusion. When generating medical images over a prolonged exposure time ( $\approx 30$  s), such as in imaging of lungs, distortions, and blur arise due to organ motion during breathing and blood supply. One of the options for image motion restoration is to apply the optical transfer function (OTF) unique to high-frequency vibrations.<sup>1</sup> In this case of medical image restoration of dynamic organs, one must deal with motion in several directions.

This paper presents results of medical image restoration of dynamic lungs, using the OTF for high-frequency vibrations. The images are shown as energy levels of detected nuclear radiation (Xe-133) inserted into the body by ventilation.

Image motion restoration refers to the problem of estimating the ideal image from blurred and noisy versions. It is well known that image restoration is an ill-posed inverse problem. That is, a unique solution may not exist and/or solution(s) may not continuously depend on the data. In solving such problems it is essential to have *a priori* information about the ideal solution. Every image restoration algorithm is based on

the observation model that establishes the relationship between the input (ideal image) and the output (observed degraded image) of the imaging system. The success of image restoration in a given application depends on how good the assumed mathematical model fits the input/output characteristics of the imaging system. In our case, where the OTF is known *a priori* or can be estimated from numerical calculations, the degraded image can be filtered in order to compensate for the degradations introduced by the limited spatial frequency of the image motion OTF. The filters are based on knowledge of the OTF and the power of the noise in the picture.

The point-spread function or the line-spread function (LSF) of image motion are the key for calculating the inverse filter for image restoration. Direct solution can be available only if they are suitably characterized. In the case where motion and therefore OTF is random such characterization can be calculated numerically in real time.<sup>1</sup> Significant improvements to idealized solutions cannot be constructed straightforwardly. In each case it is necessary to adopt an iterative approach that will converge to the true image. When this algorithm should be applied and how many iterations should be attempted can only be decided on the basis of practical computational experiments.

Address all correspondence to D. Arbel. Fax: 972-7-647-2949; E-mail: danny@eesrv.bgu.ac.il

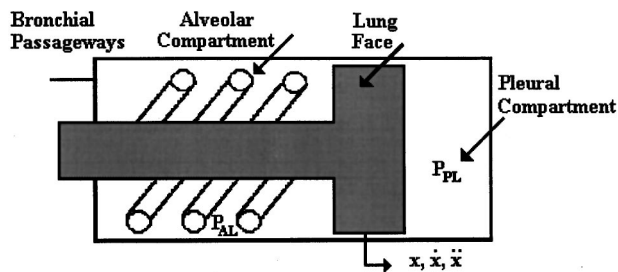


Fig. 1 Motion of lung idealized as linear actuator/piston of area  $A_l$  with spring and viscous resistance effects (after Ref. 2).

## 2 Lung Motion Description

There are two options to obtain the function of lung motion, by experiment and measurement, or by appropriate simulations based on lung motion. Our research results were compared with computer simulation packages aimed at developing the model of the human respiratory system, such as: (a) BATH/p,<sup>2,3</sup> and (b) ACSL simulation.<sup>4</sup>

### 2.1 Model of the Lung<sup>2,3</sup>

When defining lungs motion for medical image restoration, one needs to consider random motion caused by patient movement and ordinary motion caused by heart beats and respiration. We focused only on ordinary motion. The concept of a moving piston forms the basis for models of the motion and gas flow processes associated with the lungs. The operation of the lung is idealized as a linear piston of area  $A_l$  (Figure 1) with spring and viscous resistance effects. The model deals with the following effects: (1) stiffness (or elastance) of the lung and surrounding tissue, (2) variation in lung elastance, (3) alveolar pressure, (4) rate of change of alveolar lung pressure, (5) transpulmonary pressure, (6) lung dimension, (7) lung area, (8) mass of lung, (9) fractional dead volume, (10) total lung capacity, (11) functional residual capacity (FRC), (12) residual volume, (13) acceleration, (14) velocity and displacement of the lung wall, (15) air density, (16) orientation of the human, (17) Coulomb friction (hysteresis), and (18) viscous friction thoracic force.

The transpulmonary pressure, the pressure difference across the lung, is given by:

$$P_l = P_{al} - P_{pl}, \quad (1)$$

where  $P_{al}$  represents the alveolar pressure and  $P_{pl}$  intrapleural pressure, which exists inside the pleura and acts on the lung wall.

The stiffness (or elastance),  $k$  (inverse of compliance) of the lung and chest wall system consists of two distinct components, lung stiffness  $k_l$ , and surrounding tissue, i.e., ribcage, diaphragm, and pleural compartment stiffness  $k_{pl}$ . Moreover, stiffness varies considerably over the working range of the lung, from the residual volume to total lung capacity. Figure 2 shows the variation of lung volume with the transmural (differential) pressure between the alveolar and pleural compartments (marked  $L$ ), and the pleural compartment and the atmosphere (marked  $W$ ) for a normal healthy

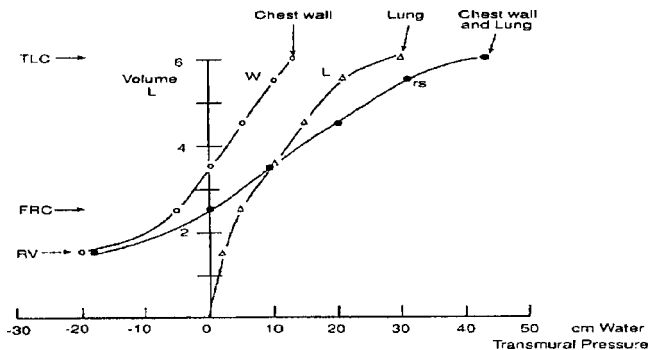


Fig. 2 Variation of lung volume with the transmural (differential) pressure between the alveolar and pleural compartments ( $L$ ), and the pleural compartment and the atmosphere ( $W$ ) for a normal healthy human (after Ref. 2).

human. The gradients of these graphs are proportional to compliance of the lung or chest wall and the reciprocals are the respective elastances<sup>2</sup>

$$f(V_l) = \Delta(P_l) / \Delta(V_l), \quad (2)$$

where  $f(V_l)$  is the variation in lung elastance ( $\Delta(P_l) / \Delta(V_l)$ ) with the lung volume  $V_l$ .

Stiffness is defined as the ratio of the rate of change of force with respect to displacement,  $\Delta(F_l) / \Delta(x)$ . This is related to elastance  $\Delta(P_l) / \Delta(V_l)$  by

$$\text{stiffness} = \frac{\Delta(F_l)}{\Delta(x)} = \frac{A^2 \cdot \Delta(P_l)}{\Delta(V_l)}, \quad (3)$$

where  $A$  is the area which is affected by the pressure in the lung.

### 2.2 Functional Residual Capacity (FRC)<sup>2,3</sup>

The FRC is the lung volume in the rest position, when the spring force due to the lung (acting on the pleural compartment) is exactly balanced by the chest wall force. The lung wall displacement  $x_f$  at FRC ( $V_f$ ) is given by

$$x_f = V_f / A_l. \quad (4)$$

At this condition, when balance between the forces occurs, alveolar pressure is equal to atmospheric pressure, and air flow from lungs is zero. At FRC, the interpleural pressure (in the pleural compartment)  $P_{p0}$  is subatmospheric,<sup>5</sup> with a typical value taken as  $-5$  cm water.

A more detailed description of the lung motion, which starts by defining the displacement in steady state and in the absence of Coulomb fictional resistance,<sup>6</sup> is presented in Refs. 2 and 3. Typical values for mass of a lung are used,<sup>7</sup> 0.5 kg being typical for a normal male.

The lung is regarded as a control volume  $V_l$  into which air flows ( $Q_l$ ) during exhalation and from which air flows during inhalation. The volume is determined from the displacement of the lung. The net flow of gas into the lungs is given by

$$Q_l = \rho \cdot A_l \frac{dx}{dt}, \quad (5)$$

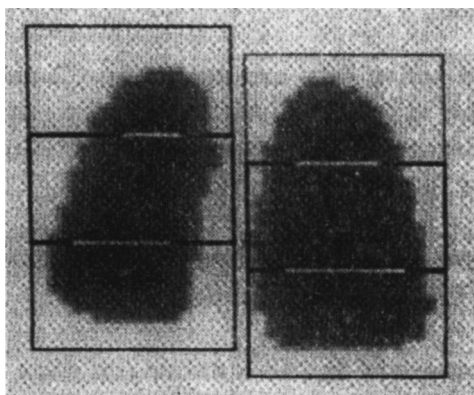


**Fig. 3** Lung segmentation of left and right lungs with three segments each.

where  $\rho$  is air density,  $A_l$  is lung area, and  $x$  is the displacement of the lung wall.

The rate of change of alveolar lung pressure is given by

$$\frac{dP_0}{dt} = \left( \frac{nRT}{V_l} \right) \cdot \frac{d(V_3 - V_l - V_{O_2} + V_{CO_2})}{dt}, \quad (6)$$

where for air  $n$  is the polytropic index,  $R$  is the gas constant,  $T$  is the temperature, and  $V_{O_2}$  and  $V_{CO_2}$  are, respectively, oxygen flow into carbon dioxide flow from the pulmonary blood.

### 3 Lung Segmentation

#### 3.1 Lobar Anatomy<sup>8</sup>

The lobar architecture of the right lung includes three lobes: (1) right upper lobe (RUL), (2) right middle lobe, and (3) right lower lobe. The RUL occupies the upper 1/3 of the right lung. The lobar architecture of the left lung is slightly different from the right. Because there is no defined left minor fissure, there are only two lobes on the left: (1) left upper and (2) left lower lobes.

In general, fissures are not readily identifiable on plain films, with only small portions typically visualized at best. This is because fissures, which are composed of only two layers of visceral pleura, may not present a significant radiographic interface and will not produce a shadow. However, if there is fluid within the pleural space or if the visceral pleura is thickened, fissures may be seen in their entirety. Neither the major nor minor fissures are definitively demonstrated on CT. In fact, because of the axial orientation of the right minor fissure, exact delineation of the border between the right middle and upper lobes is almost impossible on CT.

#### 3.2 Image Processing Segmentation

One way of handling the movement in a medical image of the dynamic lung, is by decomposing the image into several images (segments). We chose to decompose the lung image into three segments according to the lobar anatomy and a comparison of the lung to a balloon as seen in the model of the lung. The three segments are: (1) the upper region, (2) the middle region, and (3) the lower region (Figure 3).

We assumed that the upper region moves like the upper half of a balloon, the middle region moves like a cylindrical

balloon, and the lower region of the lung moves like the lower half of the balloon. This assumption simplifies the image restoration results. The additional segmentation process we developed is based on the stiffness of the lung. We chose to slice every region, where each slice is of different width (which will be used later in the OTF), according to the model of the motion of the lung. That way of handling the movement in the image reduced the distortions caused by the restoration process.

It should be mentioned that the edge of the lung, the lung wall, is not a perfectly smooth curve, so we had to use image processing algorithms to find the edges of the lungs in the image to prevent image processing of the background.

## 4 Image Motion OTF

There are two methods presented to calculate MTF for any type of motion, including random motion that cannot be characterized by any unique MTF.<sup>9,1</sup> One is based on calculation in the spatial frequency domain.<sup>9</sup> The second is based on calculation carried out in the spatial domain and yields actual OTF. The latter method is much faster so it is more suitable for practical systems that work in real time. In addition, the phase transfer function is also obtained.<sup>1</sup> We used the second method. All that is required for both methods is the function of relative image motion.

### 4.1 Spatial Frequency Domain (MTF)

The spatial frequency domain method<sup>9</sup> is based on the assumption of an object with a sinusoidal luminance pattern:

$$i(x) = B_0 + B_m \cos(2\pi fx), \quad (7)$$

where  $f$  is spatial frequency,  $x(t)$  is the motion function for spatial coordinate  $x$ , and  $B_0$  and  $B_m$  are constants.

To determine the modulation of the intensity pattern of the image it is necessary to know the relative motion  $x(t)$  between the camera and the object. When this motion is known analytically, the MTF also can be obtained analytically, as in the cases of linear motion, high-frequency vibration, or parabolic motion. For other cases when the exact analytic function  $x(t)$  is not available, it is necessary to expand this method to numerical calculation. This method works with discrete points of image motion instead of the mathematical function. The MTF is calculated for each spatial frequency separately and is obtained by measuring the modulation contrast function over a multitude of closely spaced spatial frequencies.

### 4.2 Spatial Domain (LSF)

In this section, the LSF derived from image motion transverse to the optical axis is obtained.<sup>1</sup> The MTF is derived as the modulus of the OTF or Fourier transform of the LSF, and the PTF is derived as the phase of the OTF.

Let  $x(t)$  be the relative displacement between the object and sensor beginning at time  $t_s$  and ending at time  $t_{s+1}$ , in which  $t_s$  is measured from the instant the sensor is first exposed. The LSF of the motion is the PDF or the histogram of  $x(t)$ . The intuitive explanation for this determination is the following. Image motion causes the system line spread image response to move spatially. These displacements are integrated during the exposure. Such motion can be described by

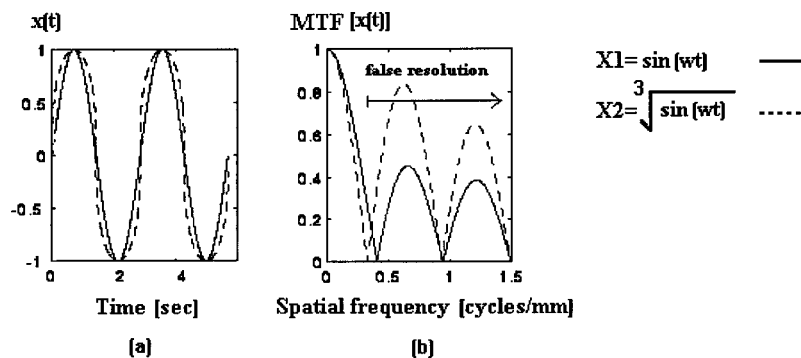


Fig. 4 Similarity between  $\sin(\omega t)$  and  $\sqrt[3]{\sin(\omega t)}$ .

a histogram of the LSF, in which frequency of occurrence of a given portion  $x(t)$  is depicted as a function of  $x$  during the time interval  $(t_s, t_s + t_e)$ . This histogram is the LSF itself. The quantity  $t_s$  is a random variable representing initial exposure time and is uniformly distributed according to  $f_t(t) = 1/t_e$ .

By decomposing the relative displacement into  $n$  monotonic parts existing in one exposure time  $t_e$ , that is,

$$t_1 + t_2 + t_3 + \dots + t_n = t_e, \tag{8}$$

the PDF is shown to be of the form

$$f_x(x) = f_t(t) \cdot \left[ \frac{1}{x'(t_1)} + \dots + \frac{1}{x'(t_n)} + \dots \right] \\ = \frac{1}{t_e} \cdot \left[ \frac{1}{x'(t_1)} + \dots + \frac{1}{x'(t_n)} + \dots \right], \tag{9}$$

$(t_s < t < t_s + t_e), \quad (d_{\min} < x < d_{\max}),$

where  $x'(t)$  is the derivative of  $x(t)$  and  $f_x(x)$  is the PDF.

The lower and the upper limits, respectively, for  $x$  are the results of the minimum and maximum displacement between the object and sensor. The PDF (or histogram)  $f_x(x)$  represents the LSF. The LSF is equal to  $f_x(x)$  and the OTF is the one-dimensional (1D) Fourier transform of the LSF:

$$\text{OTF}(f) = \int f_x(x) e^{-j2\pi f x} dx, \tag{10}$$

where  $f$  is spatial frequency.

Thus, LSF for image motion can be determined from a histogram of the motion, and the resulting OTF for such motion is given by Eq. (10).

### 4.3 Image Degradation by Sinusoidal Vibration

Sinusoidal vibration is a very critical factor in dynamic imaging systems. The sinusoidal motion can be prevented in principle by proper design; in practice, however, it is often the most serious image motion. Degradation of image quality as a result of sinusoidal motion<sup>10</sup> depends on the ratio of exposure time  $t_e$  to the period of the sinusoidal motion  $T_0$ . In this case, it is necessary to distinguish between two categories.

1. **High-frequency Vibration** in which the exposure period is long compared to the period of the simple harmonic

motion ( $t_e \geq T_0$ ). The LSF for this motion is given by the histogram of the sine function over one period. The exact calculation appears in Ref. 1, and the result is

$$\text{LSF}_{\text{HF}} = 1/[\pi(D^2 - x^2)^{1/2}], \quad |x| < D, \tag{11}$$

where  $D$  is the maximum vibration amplitude. The MTF for this case is given by the Fourier transform of Eq. (11):

$$M_s(f) = J_0(2\pi f D), \tag{12}$$

where  $J_0$  is the zero-order Bessel function. The PTF for the ideal case is equal to zero because the LSF is an even function. It is important to mention that the result in this case remains the same for  $t_e \geq T_0$ . The blur radius is still the peak-to-peak displacement  $2D$  as long as  $t_e \geq T_0$ .

2. **Low-frequency Vibration** in which the exposure period is short compared to the vibration period ( $t_e < T_0$ ). Quantification of the low-frequency vibrational image blur radius  $d$  is much more complicated, however, because it depends on the initial phase of the oscillatory motion as well as on the instant and duration of the time exposure, both of which are often random processes. The influence of the MTF degradation is much more severe than that of the PTF; therefore, the following discussion concentrates only on the MTF.

### 4.4 Degradation Process of High Frequency Vibration

For the case of high-frequency vibration, for sinusoidal movement, the amplitude of the vibration is peak-to-peak displacement  $d = 2D$ . In this case, the MTF is the well-known zero-order Bessel function  $J_0(2\pi f D)$ . The first zero of this function occurs at  $f_{r\max} = 0.7655/d$ . The width of the MTF is smaller than in the cases of linear motion or acceleration motion, so most degradation occurs in the case of high-frequency vibration. These results are obtained for any constant blur radius. However, they are not valid for constant time exposure.<sup>1</sup>

In the case of lung image restoration, we should notice that the lungs volume changes sinusoidally,<sup>4</sup> but the displacement in one direction is the third root of the volume (in a sphere), and the square root of the volume (in a cylinder). It means that we had to find the OTF for those functions. In practice, we decided to use the zero-order Bessel function, because of the similarity until the first zero as can be seen in Figure 4. In our experiment, described in Sec. 5, the assumption of using

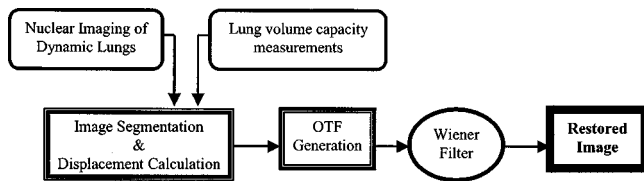


Fig. 5 Block diagram of imaging system and restoration.

OTF based on high frequency vibration is correct, especially for prolonged exposure time of 300 s which is much longer than the breathing vibrational cycle.

## 5 Experimental Description and Results

We divided the experiment into four stages: (1) generation of signals of lung volume capacity in respiration assisted by BREEZE software combined with the lung ventilation medical system, (2) dynamic scan lung ventilation nuclear images, and signals of lungs, generated by the ‘Elscent APEXView V4.00A’ medical systems, (3) image segmentation, and (4) image restoration using motion OTF (see Figure 5).

The experimental stages are based on the simulation results, which are given in the literature.<sup>2–6</sup> The results and the conclusions in Refs. 2–6, are similar to the actual results for the medical systems. For image restoration purposes it is always better to use actual displacement measurements obtained from a sensor attached to the patients’ body instead of motion estimation tools. Usually, estimation results are used when there are no actually measured data. However in our case the medical system produced the specific characterization of the organ motion. On the other hand, if measurements could not be acquired in parallel to the image scan, it is recommended that you use an average signal based on several measurements.<sup>11–13</sup>

### 5.1 Generated Signals Images and Segmentation

With BREEZE software combined with the lung ventilation medical system, we measured the volume capacity versus time lung ventilation signals. One sample is shown in Figure 6. It is clear that the ventilation signals are essentially sinusoidal, as suggested in respiratory physiology literature.<sup>2–4</sup> It can be seen that there is a visual decline in the signal, which is due to the measurement system. However, we succeeded in correcting this problem by subtraction of the linear dc slope. We can see that the volume amplitude varies over a range of about 2 L. This point is very important in calculating the displacement of the lung wall (see Sec. 4.4). For lung image

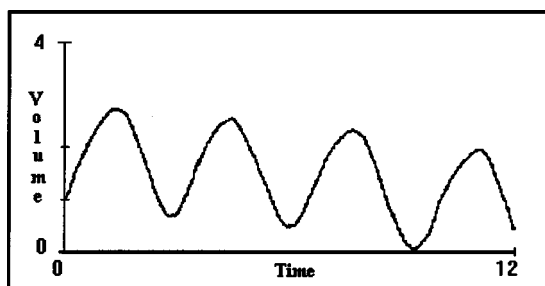


Fig. 6 Measured signal of respiration.

restoration, because of the prolonged exposure time, we deal with high-frequency vibration, so we need only the amplitude and may ignore the frequency. We can derive the amplitude from the volume capacity signals, and this is one way to obtain the amplitude parameter for the OTF formed by zero-order Bessel function  $J_0$ .

To simplify the restoration process we divided the image into three segments, assuming that the upper segment has the shape of a dome, the middle segment has a shape similar to a cylinder, and the lower segment has an upside dome shape. Each segment was restored separately, the upper and the lower segments were restored by using the radial MTF, and the middle part was restored using the MTF along the  $x$  and  $y$  axis. The restoration process described above, deals only with the lung image that was extracted from the surrounding background.

The following are recommended camera parameter settings (400 mm field of view) for Xenon-33: (1) acquisition—dynamic, (2) pharmaceutical—xenon-133 gas, (3) energy—78 keV, (4) frame size—64×64, (5) zoom—1.

Figure 3 shows an example of lung segmentation, in which the generated image is decomposed into three segments.

### 5.2 Image Restoration Using Wiener Filter Based on High-frequency Vibration OTF

The exposure time for generating an image is very long (30 s and even more). Since this is much longer than the breathing cycle, it was appropriate to choose OTF based on high-frequency vibration. This was inserted into the Wiener filter

$$\text{Wiener} = \text{OTF}^* / (|\text{OTF}|^2 + 1/\text{SNR}), \quad (13)$$

where the signal-to-noise ratio (SNR) is a constant estimated value, and the OTF is the zero-order Bessel function [Eq. (12)] limited to  $f_{r\max} = 0.7655/d$ . We obtain the displacement  $D$  ( $D = d/2$ ) by calculations or measurements. The medical imaging system finds the displacement in real time through the imaging process. Two options for calculations are (1) to derive the displacement from the measured volume of the lungs or (2) to scan the logarithm of the fast Fourier transform of the original vector where zero points occur. The displacement  $D$  is the displacement between two zeros.<sup>14,15</sup>

### 5.3 Results

The following figures show the restored images using a Wiener filter based on the zero-order Bessel function MTF and the numerical MTF derived from the actual motion obtained from the motion sensor. Notice we deal only with the object close to the edges. The image size is 128×128 pixels. Calculations indicate a blur of 4–5 pixels. As presented in Figures 7 and 8, the energy of the radiation is spread around the center of the lung. We should remember that we deal with images generated by isotopic radiation, and the image is being shown as energy levels of radiation. Consequently, we expect to focus all the spread energy into the center of the image where most of the radiation is.

Figures 7(a1) and 8(a1) present the original images of the left and right lungs followed by the restored image using the zero Bessel function as the MTF [Figures 7(b1) and 8(b1)], and the restored images from the numerical MTF [Figures 7(c1) and 8(c1)]. Figures 7(a2), 7(b2), 7(c2), 8(a2), 8(b2), and

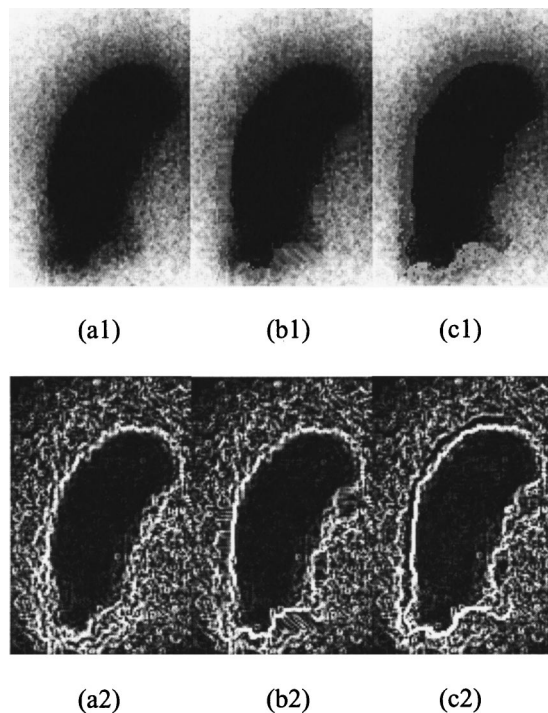


**Fig. 7** Sample of image restoration of dynamic left lung; (a1) original image, (b1) restored image using the zero Bessel function as the MTF, (c1) restored image using the numerical MTF, (a2) edge pattern of (a1), (b2) edge pattern of (b1), and (c2) edge pattern of (c1).

8(c2) represent the edges of the original and the restored images, respectively. The edges of the medical image have a significant rule in helping us recognize defects in the investigated organ. In a normal lung the blood reaches all the blood vessels in the organ. Consequently, the radiative material carried by the blood is radiated approximately uniformly from the whole organ. As a result, the obtained image has a continuous shape (as presented in Figures 7 and 8). On the other hand, in a lung with a defect the blood cannot reach all the blood vessels. As a result, the obtained image may have white spots close to the edges and/or brighter gray level spots in the inner boundary (proximal parts) of the lung, representing the defected areas. In Figures 7(b), 7(c), 8(b), and 8(c) the restoration results seem less successful in the inner boundary of the lung, where all the energy of the radiation is concentrated. It is important to clarify that the success in blur restoration is the same in the whole organ. Despite the visual evidence of success in edge restoration only, there is a chance to see good restoration results in cases with inner boundary defects (areas with different gray level spots). The enhanced edges in the restored images emphasize the defect area in the lung. Therefore, it is very important to obtain a very sharp image with enhanced edges. The benefits of our method and the suggested algorithm are improvement of the imaging system and consequently of the medical images generated, reduction in the need for other medical systems, and assistance to doctors in making better diagnoses and decisions. Clinical interpretations also become more objective and more sensitive to ventilation dysfunction since there are no longer variations in regional lung volume and image intensity, which tend to reduce the accuracy of visual estimates or regional ventilation.

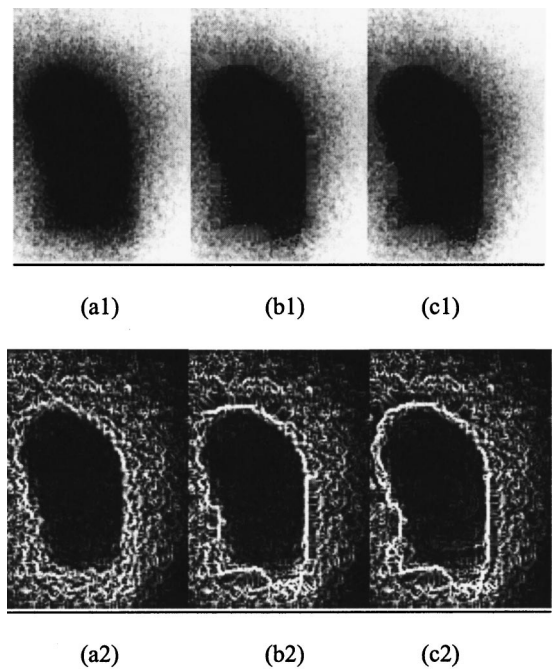


**Fig. 8** Sample of image restoration of dynamic right lung; (a1) original image, (b1) restored image using the zero Bessel function as the MTF, (c1) restored image using the numerical MTF, (a2) edge pattern of (a1), (b2) edge pattern of (b1), and (c2) edge pattern of (c1).

The better the restoration of the hardware, the greater the number of pixels affected by motion blur. The techniques described here<sup>16</sup> can be expected to be even more useful as hardware imaging technology improves to yield images with larger numbers of pixels.

## 6 Conclusions

Using motion OTF for medical image restoration of dynamic organs is a way to improve the quality of the image, and a way to simplify the diagnosis for doctors. We suggest a new method, which permits considering the motion in several directions simultaneously. If we know the motion parameters, we can easily find the appropriate OTF for the image restoration. Otherwise, we can scan and look for the right parameters by relying on the object motion model. For the latter, it is still a prolonged process (about 3 min). In this experiment we used  $64 \times 64$  pixel images. It is difficult to improve such an image noticeably with a short vector, less than 30 pixels, because the blur is no more than 2–3 pixels. Nevertheless, in Figure 7 the restoration process noticeably improves restoration of the lung center area. As hardware technology improves, motion blur should affect a greater number of pixels, and the technique described here should be even more useful, as they already have shown to be for nonmedical imaging.<sup>16</sup>

Another aspect is the definition of image quality. In searching for the right parameters, we must instruct the image processing system as to which image is best. The use must be qualified and trained to choose the best image restoration. In the future it may be possible, assisted by detection and identification systems, to choose the best result. Meanwhile, we can implement our restoration algorithm in real time, using medical systems that measure all the needed parameters, such

as the motion amplitude, and combine the image processing algorithm with the image processing software in the system.

In isotopic medical images, there is limited medical information for diagnosis. Doctors still have to be assisted by other medical systems. Quantitative analysis overcomes problems of visual image interpretation caused by differences in regional lung volume or tracer equilibration. The benefits of our method and the suggested algorithm are in improving the imaging system and consequently the medical images generated, reducing the need for other medical systems, and assisting the doctors to make better diagnoses and decisions. Clinical interpretations also become more objective and more sensitive to ventilation dysfunction since there are no longer variations in regional lung volume and image intensity, which tend to reduce the accuracy of visual estimates of regional ventilation.

### Acknowledgments

The authors are grateful to the Isotopic and the Lung Departments at Soroka Medical Center in Beer-Sheva.

### References

1. O. Hadar, I. Dror, and N. S. Kopeika, "Imaging resolution limits resulting from mechanical vibrations, Part IV: Real-time numerical calculation of optical transfer functions and experimental verification," *Opt. Eng.* **33**, 566–578 (1994).
2. S. P. Tomlinson, D. G. Tilly, and C. R. Burrows, "Computer simulation of the human breathing process," *IEEE Eng. Med. Biol. Mag.* **13**(1), 115–124 (1994).
3. C. W. Richards, D. G. Tilley, S. P. Tomlinson, and C. R. Burrows, "BATH/p—a second generation simulation package for fluid power system," in *Proc. 9th Int. Conf. Fluid Power*, pp. 25–27, 315–322, Cambridge, UK (April 1990).
4. B. Vielle and G. Chauvet, "An ACSL simulation of the respiratory system," *Int. J. Bio-Med. Comput.* **33**(1), 45–54 (1993).
5. N. S. Balfour and L. H. Hamilton, *Respiratory Physiology*, 5th ed., pp. 65–81 (1987).
6. S. P. Tomlinson, "The hydraulic automatic simulation package," *Modeling and Simulation Aspects*, pp. 60–64, University of Bath Press, Bath, UK (1987).
7. J. E. Cotes, *Lung Function. Assessment and Application in Medicine*, 4th ed., pp. 345–347 (1979).
8. B. H. Thompson and L. Williams, Electric Differential Multimedia Lab, City?, Iowa (1994).
9. O. Hadar, M. Fisher, and N. S. Kopeika, "Image resolution limits resulting from mechanical vibrations, Part III: numerical calculation of modulation transfer functions," *Opt. Eng.* **31**(3), 581–589 (1992).
10. D. Wulich and N. S. Kopeika, "Image resolution limits resulting from mechanical vibrations," *Opt. Eng.* **26**(6), 529–533 (1987).
11. A. Stern and N. S. Kopeika, "General restoration filter for vibrated image restoration," *Appl. Opt.* **37**(2), 7596–7603 (1998).
12. A. Stern and N. S. Kopeika, "Optical transfer function analysis of images by non-harmonic vibrations characterized by their power spectrum density," *J. Opt. Soc. Am. A* **16**, 2200–2208 (1999).
13. A. Stern, E. Kempner, A. Shukrun, and N. S. Kopeika, "Restoration and resolution enhancement of a single image from a vibration-distorted image sequence," *Opt. Eng.* **39**(9), 2451–2457 (2000).
14. R. Fabian and D. Malah, "Robust identification of motion and out-of-focus parameters from blurred and noisy images," *CVGIP: Graph. Models Image Process.* **53**(5), 403–412 (1991).
15. A. M. Tekalp, H. Kaufman, and J. W. Woods, "Identification of image and blur parameters for the restoration on noncasual blurs," in *Proc. ICASSP-85*, pp. 656–659, Tampa, FL (1985).
16. N. S. Kopeika, *A System Engineering Approach to Imaging*, SPIE Bellingham, WA (1998).